

Comparison of grid Euler deconvolution with and without 2D constraints using a realistic 3D magnetic basement model

Simon E. Williams¹, J. Derek Fairhead², and Guy Flanagan³

ABSTRACT

We describe the application of a 2D-constrained grid Euler deconvolution method which is able to determine for each solution window whether the source structure is two dimensional, three dimensional, or poorly defined and to estimate the source location and depth. In each solution window, eigenvalues and eigenvectors are derived from the Euler equations and compared to threshold levels. A single eigenvalue below the given threshold and lying in the $x-y$ -plane is shown to indicate a 2D source, while the absence of such an eigenvalue indicates a 3D source geometry. Two small eigenvalues indicate the field in the window has no distinct source. Applying these criteria to each solution window allows us to generate a map of source-geometry distribution.

We evaluate the effectiveness of 2D-constrained grid Euler deconvolution using synthetic magnetic data generated from a 3D basement model based on real topography from an area with surface-exposed faulting. This modeling strategy provides a complex, nonidealized data set that compares Euler depth estimates directly to the known basement surface depth. Our results indicate that noninteger structural indices can be the most appropriate choice for some data sets, and the 2D-constrained grid Euler method images magnetic basement structure more clearly and unambiguously than the conventional grid Euler method.

INTRODUCTION

The analysis of potential field data is an important tool for studying basement structure in hydrocarbon exploration

settings. Numerous techniques, reviewed in detail by Gunn (1997), have been developed to aid the interpretation of such data. These include Werner deconvolution (Werner, 1953), the Naudy method (Naudy, 1971), spectral analysis (Spector and Grant, 1970), and methods based on the analytical signal (e.g., Roest et al., 1992). The methods tested in this study are variants of grid-based Euler deconvolution. The original grid Euler method, referred to here as conventional grid Euler deconvolution, was proposed by Reid et al. (1990) and has become a widely used interpretation tool.

Two problems commonly arise when using conventional grid Euler deconvolution. First, it is necessary to subjectively choose a structural index value before generating the results, the chosen value depending on the type of structures expected in the study area (for example, relative abundance of contacts, dikes, and vertical pipes). Second, solutions are generated at all operator window locations, thus producing as many spurious or poorly constrained solutions as reliable ones.

The use of an incorrect structural index N over a structure will generate an incorrect depth estimate. In a given study area, the structures causing the field are unlikely to all be of the same geometrical form, so the use of a single N value is likely to be inadequate for the whole area. Several authors suggest methods for automatically selecting the structural index on a window-by-window basis. Hsu (2002) attempts to estimate source depth and structural index simultaneously by using second-order derivatives and assuming no gradient in the background field. Barbosa et al. (1999) show that such a simultaneous estimation of depth and N is invalid, since the terms are linearly dependent. Instead, they use the correlation between the observed anomaly and the estimated background level B as an indicator of the correct structural index. This method implicitly requires that individual anomalies be isolated to determine the correlation. Nabighian and Hansen (2001) and Phillips (2002) utilize the Hilbert transform components of the original field to solve

Manuscript received by the Editor May 1, 2003; revised manuscript received August 30, 2004; published online May 23, 2005.

¹University of Leeds, School of Earth Sciences, Leeds LS2 9JT, United Kingdom. E-mail: simonw@earth.leeds.ac.uk.

²GETECH, University of Leeds, Leeds LS2 9JT, United Kingdom. E-mail: jdf@getech.com.

³ConocoPhillips, Regional Gravity and Magnetics, 3020 Permian Building, 600 North Dairy Ashford, Houston, Texas 77079. E-mail: guy.flanagan@conocophillips.com.

© 2005 Society of Exploration Geophysicists. All rights reserved.

additional Euler equations and to solve for both depth and structural index in two separate steps.

Euler solutions can be interpreted without rejecting any solutions by relying heavily on the skill of the interpreter to discriminate between reliable and spurious solutions. A more mathematically rigorous technique to discriminate between reliable and spurious solutions is preferable, such as the use of estimates of the standard deviations of model parameters from the least-squares inversion (Thompson, 1982). The standard deviation is often expressed as a percentage of the calculated depth, since deeper structures would be expected to give solutions that have relatively large absolute errors but are still useful. Laplacian Euler deconvolution (Fairhead et al., 1994) saves computation time and reduces spurious solutions by only calculating solutions for window locations where the total horizontal derivative has positive curvature. Mushayandebvu et al. (2001) introduce a second 2D Euler equation, described as a rotational constraint, thereby allowing the computation of two Euler solutions for each window; solutions are considered reliable when the two sets of equations give spatially consistent results. Nabighian and Hansen (2001) develop this idea and show that it can be extended to grid data, and that the extended grid Euler algorithm is a generalization and unification of the Euler and Werner methods.

The 2D-constrained grid Euler method goes some way toward solving these problems by using only the conventional Euler equation and allowing a means of distinguishing between solution windows where the source is two dimensional, three dimensional, or poorly defined, without the need to introduce extra equations. An objective of our study is to analyze this method and compare the results with conventional Euler deconvolution.

Previous testing of the effectiveness of a potential field interpretation method has generally relied on either using simple models consisting of contacts, dikes, or simple polygons in groups or in isolation or using real data sets where the distribution of source structures is inferred from the interpreted results. In the first case, the model solutions can be shown to be correct, but the models are highly idealized and not necessarily good approximations to real geology. In the second case, the accuracy of the derived solutions is uncertain because of little or no ground-truthing. Thus, there is an important gap in understanding between the results of interpretation techniques for idealized models and the ultimate goal of interpreting field data reliably. This study attempts to fill that gap.

We propose a new approach where a 3D basement model is used to test the effectiveness of potential-field inversion techniques. Real topography data have been used as the surface of a magnetic basement with uniform magnetization, overlain by nonmagnetic sediments. From this surface various forward-modeled grids of the induced magnetic response can be generated for any inclination and declination. The synthetic data have the complexity of field data from a real basin environment and are generated from a known model, allowing us to compare the results of any given inversion strategy with the correct answer.

First, we describe the methodology for conventional and 2D-constrained grid Euler deconvolution; then, we demonstrate a new procedure for parameterizing the 2D-constrained grid Euler method — a step crucial for obtaining reliable solutions — using a simple synthetic model. Next, we intro-

duce the 3D basement model derived from real topography data and describe the 2D-constrained grid Euler parameterization process for complex data sets. Finally, the results of applying both conventional and 2D-constrained grid Euler method on the 3D test model are presented and discussed. Our results indicate that noninteger structural indices can provide the best depth estimates for some data sets and that the 2D-constrained grid Euler method images magnetic basement structure more clearly and unambiguously than conventional grid Euler deconvolution.

METHODOLOGY

Grid Euler deconvolution

The application of Euler deconvolution as a potential-field interpretation tool has seen several significant advances since the work of Thompson (1982). The original profile or 2D method is adapted for use as a grid-based method by Reid et al. (1990), who give the conventional 3D Euler deconvolution equation as

$$(x - x_o) \frac{\partial T}{\partial x} + (y - y_o) \frac{\partial T}{\partial y} + (z - z_o) \frac{\partial T}{\partial z} = N(B - T), \quad (1)$$

where (x_o, y_o, z_o) is the position of the top of the source (or the geometric center for 3D sources), (x, y, z) is the location of the field measurement, T is the total magnetic intensity (TMI) anomaly value, B is the background field, and N is the structural index. Conventional grid Euler deconvolution in this form has become a widely used interpretation technique. For each window with n data points, equation 1 is written for one to n data points in the matrix form $\mathbf{Am} = \mathbf{d}$:

$$\begin{bmatrix} \frac{\partial T}{\partial x_1} & \frac{\partial T}{\partial y_1} & \frac{\partial T}{\partial z_1} & N \\ \vdots & \vdots & \vdots & \vdots \\ \frac{\partial T}{\partial x_n} & \frac{\partial T}{\partial y_n} & \frac{\partial T}{\partial z_n} & N \end{bmatrix} \begin{bmatrix} x_o \\ y_o \\ z_o \\ B \end{bmatrix} = \begin{bmatrix} x_1 \frac{\partial T}{\partial x_1} + y_1 \frac{\partial T}{\partial y_1} + z_1 \frac{\partial T}{\partial z_1} + NT_1 \\ \vdots \\ x_n \frac{\partial T}{\partial x_n} + y_n \frac{\partial T}{\partial y_n} + z_n \frac{\partial T}{\partial z_n} + NT_n \end{bmatrix}, \quad (2)$$

where $\partial T/\partial x_1$ is the partial derivative of T with respect to x evaluated at $x = x_1$.

Equation 2 is solved as an overdetermined least-squares problem to obtain the four unknowns x_o , y_o , z_o , and B , where the window size commonly ranges from 4×4 to 10×10 grid-points. The operator window steps across a grid of data, calculating individual source locations brought together to form a map of source distribution.

2D-constrained grid Euler deconvolution

In this study, we attempt to better understand the 2D-constrained grid Euler method, originally proposed by Mushayandebvu et al. (2004). The method distinguishes between 2D and 3D sources by analyzing the eigenvalues and eigenvectors of the Euler normal equations matrix ($\mathbf{A}^T \mathbf{A}$, where \mathbf{A} is as given in equation 2 for each window. Within a data set, the reduced-to-the-pole (RTP) magnetic anomalies over each 2D source (e.g., faults, dikes) are also two dimensional, parallel to the structures. The data within solution windows over these sources will be strongly two dimensional, creating a linear dependence between the columns containing the horizontal gradients in the Euler \mathbf{A} matrix. Matrix $\mathbf{A}^T \mathbf{A}$ will have an eigenvector that points along strike and whose associated eigenvalue has a very small value (since the rate of change of the field in this direction is negligible) and thus can be recognized. Equation 2 is then solved by eigenvector expansion, using a structural index appropriate for a 2D source (e.g., 0 for a contact, 1 for a dike). Having determined the 2D source strike direction, the dip, and susceptibility, we can also compute contrast, assuming either a contact or dike model (Mushayandebvu et al., 2001).

For solution windows where the source geometry is not two dimensional, the source type can still be determined. Where no source is present, the gradient of the field is effectively zero in all directions; hence, two eigenvalues are below the threshold and lie in the x - y -plane. By contrast, no small eigenvalues

in the x - y -plane are observed over 3D structures. In windows where no source is present, no solution is calculated (providing a mechanism to reject poor solutions), while solutions for 3D sources are calculated by the conventional Euler deconvolution using a structural index appropriate for 3D sources (e.g., two for a vertical pipe, three for a sphere).

The full solution strategy is summarized in Figure 1. Application of the 2D-constrained grid Euler method to real data sets is not straightforward. Real data contain noise, and geological structures (e.g., faults and dikes) are rarely perfectly two dimensional. Thus, we cannot merely look for zero eigenvalues; we must allow for a certain noise level (which varies between data sets) so that 2D features will be associated with a very small eigenvalue (small relative to the largest eigenvalue for that solution window and to the smallest eigenvalues elsewhere in the data set) whose corresponding eigenvector is almost parallel to the x - y -plane. To do this, we must set two thresholds: one to decide how large an eigenvalue can be and still be considered to indicate an effectively zero gradient in the field (the eigenvalue threshold) and a second one to determine whether the corresponding eigenvector lies in the x - y -plane (the x - y -plane threshold). The x - y -plane threshold value is compared to the sum of the elements in the eigenvector corresponding to the eigenvector components along the x - and y -directions. This sum can have a maximum of one. The closer the sum is to one, the closer the eigenvector is to the x - y -plane (eigenvectors are normalized such that the vector sum of all four elements is one).

SIMPLE MODEL EXAMPLE

The concepts described above are demonstrated visually using synthetic data from a simple model (Figure 2). Figures 3a and 3b show the spatial variation in magnitude of the smallest and second smallest eigenvalues determined from the Euler $\mathbf{A}^T \mathbf{A}$ matrix for each window of the grid, using a window size of 5×5 gridpoints. Figures 3c and 3d show the variation of the x - and y -component sums calculated from the corresponding eigenvectors. These plots illustrate the different nature of

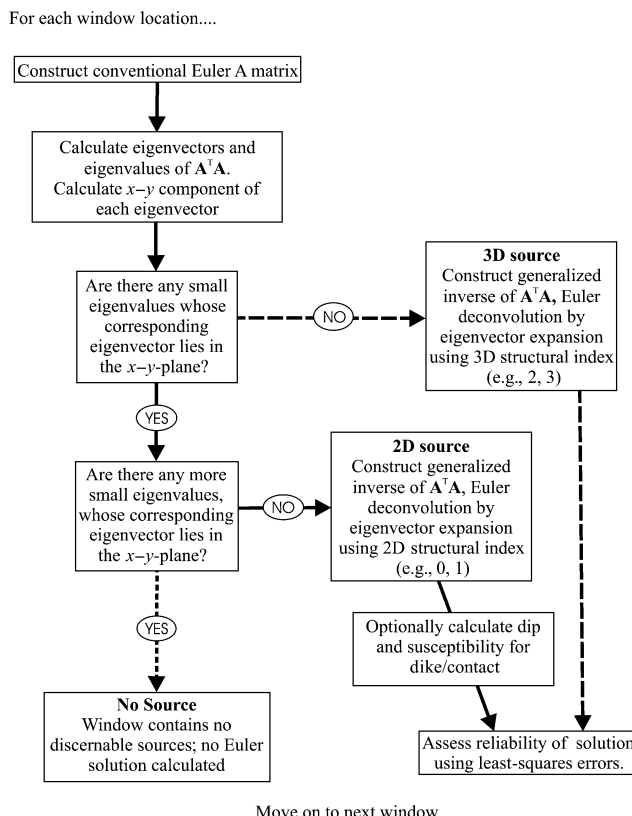


Figure 1. Solution strategy flowchart for 2D-constrained grid Euler deconvolution. Solid arrows show the path that will indicate a 2D source.

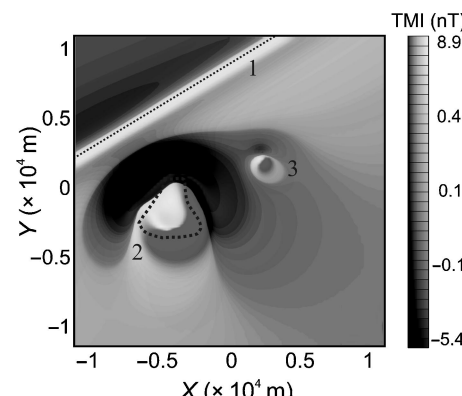


Figure 2. TMI for a simple model, consisting of (1) a 1000-m-deep, 100-m-wide dike, (2) a 1000-m-deep, 100-m-thick sill (edge denoted by dashed line), and (3) a vertical pipe at depth 400 m with a diameter of 100 m. Grid cell size is 250 m, and magnetization is induced by a geomagnetic field whose strength is 50 000 nT, inclination is 45°, and declination is 0°. Susceptibility of each source is 2.5×10^{-4} cgs (3.1×10^{-3} SI).

eigenvalues over 3D structures, 2D structures, and areas with no nearby sources. By correctly defining the threshold parameters (in this case, an eigenvalue threshold of 1×10^{-7} and an x - y -plane threshold of 0.7), we can map these different source geometries.

Over structures that are unambiguously three dimensional, we see areas of values higher than the threshold on the plots of both the smallest (Figure 3a) and second smallest eigenvalues (Figure 3b). Over areas containing 2D structures, such as the dike, only one eigenvalue is smaller than the threshold (compare Figures 3a and 3b), lying on the x - y -plane (Figure 3c).

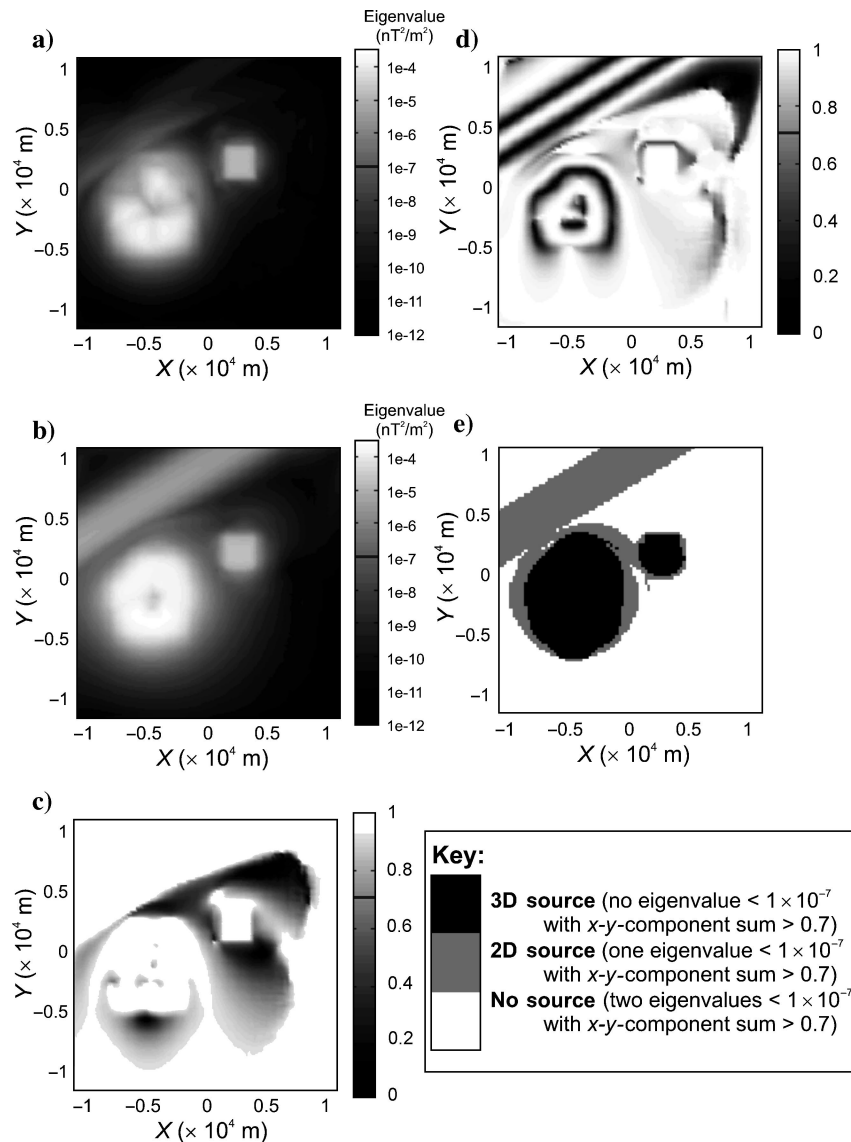


Figure 3. Spatial distribution of eigenvalues and eigenvectors of a Euler $\mathbf{A}^T\mathbf{A}$ matrix for the simple model in Figure 2 and their use. (a) Smallest eigenvalue. (b) Second smallest eigenvalue. (c) Sum of x - and y -components of the eigenvector corresponding to the smallest eigenvalue. (d) Sum of x - and y -components of the eigenvector corresponding to the second smallest eigenvalue. (e) Spatial distribution of inferred structure type (3D, 2D, no source) in each window based on data in Figures (a)–(d) and the strategy shown in Figure 1, using an eigenvalue threshold of 1×10^{-7} and an x - y -plane threshold of 0.7 (threshold levels are indicated in color scalebars of (a)–(d)). Black areas indicate windows with 3D sources, gray indicates 2D sources, and white indicates no source.

Over the center of the sill, both eigenvalues are larger than the threshold; while over the edges, one eigenvalue is below the threshold and lies in the x - y -plane. Hence, the implied geometry is three dimensional over the center of the sill but two dimensional around the border. The spatial extent of the sill is sufficiently small relative to the window size so that it appears three dimensional to windows over its center. Away from the center, however, the smallest eigenvalue decreases, indicating the 2D nature of the edge. In areas where no sources are present, two eigenvalues are below the threshold, lying in the x - y -plane.

The information in Figures 3a–d can be used to produce a single plot, which shows the distribution of different types of solutions (e.g., 2D, 3D, no source) for any given set of threshold values. Figure 3e shows the distribution of source types inferred by applying the strategy outlined in Figure 1, with the threshold levels quoted above.

The eigenvalue and x - y -plane thresholds must be chosen before source solutions can be calculated, and their best values vary from one data set to another. For this reason, the process is divided into two steps. The first step involves calculating and plotting the spatial variation of the eigenvalues and eigenvectors across the data to determine threshold parameters. In the second step, these parameters are used during the calculation of source depths.

A REALISTIC BASEMENT MODEL

An aim of this study is to use a realistic basement model to test different Euler deconvolution methods. To discuss the application of the methodology to this model, we must first introduce the model itself. This section describes the modeling strategy, followed by an explanation of the parameterization process for 2D-constrained grid Euler deconvolution.

3D test model derived from real topography

The original digital elevation model used is a 30-m-spaced universal transverse mercator (UTM) grid covering a 10.5×10.5 -km area of the Volcanic Tablelands, north of Bishop, California (the coordinates of the center of the original area are $37^{\circ}28' N$, $118^{\circ}25' W$). The area was chosen because it contains a variety of structures: two relatively long, large-offset faults (striking north-south and east-west), en echelon arrays of smaller scale north-south faults, transfer zones between faults, and an unfaultered deep basin area in the southeast corner.

To convert the topography into a 3D test model representative of basin-scale

magnetic basement surface, the digital elevation model was increased in scale by a factor of 30 in all three dimensions, under the assumption that faulting patterns are fractal. This gives an elevation model (Figure 4) for an area measuring 315×315 km. The topographic surface datum was then shifted such that the highest point has a depth of a few hundred meters below datum (zero) and the deepest point has a depth just less than 10 000 m.

This topographic surface has been taken as the top of the magnetic basement with a constant susceptibility, assumed to extend to 20 000 m depth and be overlain by nonmagnetic sediments. A laterally extended version of this 3D test model was used to simulate the TMI response for a range of geomagnetic field inclinations. Figure 5 shows the magnetic response for a basement susceptibility of 1×10^{-3} cgs units (1.26×10^{-2} SI units) and an ambient geomagnetic field with strength of 50 000 nT, inclination of 45° , and declination of 0° . Gaussian noise with a zero mean and a standard deviation of 0.2 nT has been added, and the data were filtered using a Hanning low-pass operator. RTP was applied to the data before the Euler solutions were generated, a step demonstrated as being necessary by Williams et al. (2003).

Additional complexity could be introduced to the model. For example, we could add different types of noise (e.g., acquisition, gridding of variably spaced profiles), variations in basement remanence and susceptibility, or interference caused by the presence of intrasedimentary and basement magnetic bodies. However, for this study a simple basement model scenario is used where the synthetic data are generated with a single susceptibility.

For comparison purposes, all parameters in the Euler deconvolution have been kept the same unless otherwise stated. The window size is 10×10 gridpoints (9 × 9 km).

Parameterization

The first step in 2D-constrained grid Euler deconvolution is to calculate the eigenvalues and eigenvectors of the Euler nor-

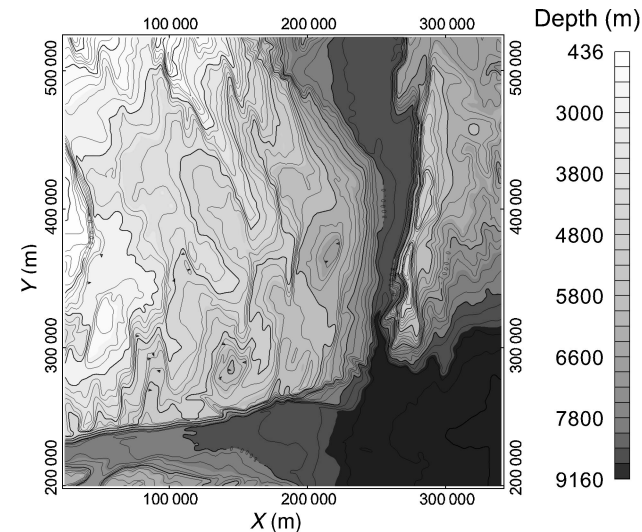


Figure 4. Depth to basement obtained from the topography from the Bishop study area after being upscaled by a factor of 300 in all dimensions and then dc shifted downward to make the highest point a few hundred meters below the zero datum. Contour interval is 200 m.

mal equations matrix $\mathbf{A}^T \mathbf{A}$ for each window. The relevant values are plotted in Figures 6a–d (in the same format as Figures 3a–d); however, determining the best parameterization from these plots is difficult because of the interrelation of these two threshold parameters. Figure 6e shows this distribution of different types of solutions (i.e., 2D, 3D, no source) for an eigenvalue threshold of 3×10^{-7} and an x - y -plane threshold of 0.7. The choice of threshold values is justified in the following paragraphs.

The eigenvalue threshold should be small, but how small? The range of eigenvalues across Figure 6a varies by several orders of magnitude; but we can see that the smallest eigenvalues are fairly small everywhere except for a few isolated spots (indicating possible 3D sources), while the second smallest eigenvalue shows a clear correlation with the main 2D structures in the model. These eigenvalues are generally greater than 8×10^{-7} over the 2D sources and less than 2×10^{-7} elsewhere; thus, a good eigenvalue threshold would be somewhere between these two values. Once this narrow range has been defined, the final value is picked to give the most coherent, geologically plausible pattern of 2D and 3D structure areas.

The x - y -plane threshold value must be in the range of 0 to 1. Theory suggests a high threshold is desirable, so we only consider structures to be two dimensional when the smallest eigenvalue is very close to the x - y -plane (for example, in Figures 3c and 3d the vector sum over the dike is >0.99). However, once again we must allow for noise (in this case numerical noise, random noise added to the data, and noise from nonidealized sources). Such a high x - y -plane threshold value results in strands of 2D solutions in parts of the data where the 3D model is relatively featureless (these results are not shown). In such no-source areas there are two small eigenvalues, but one of the corresponding eigenvectors is perturbed

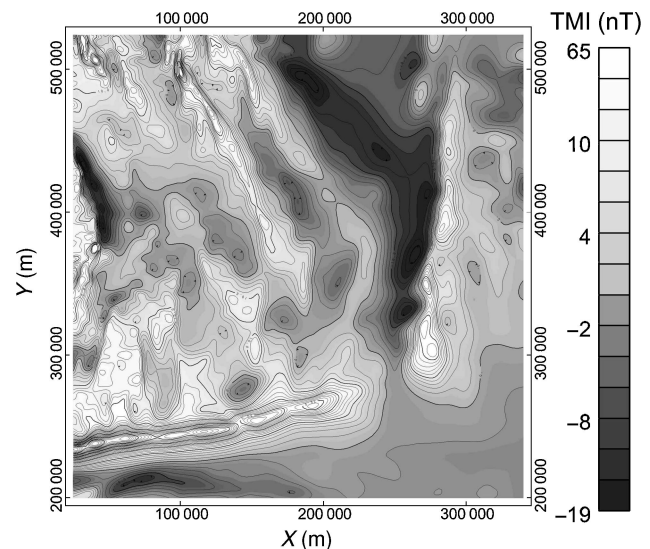


Figure 5. Synthetic magnetic anomaly field of the topography in Figure 4, assuming induced magnetization in the basement below the surface [basement susceptibility is 1×10^{-3} cgs units (1.26×10^{-2} SI units)] and no magnetization above it. Ambient field has strength of 50 000 nT, inclination of 45° , and declination of 0° . Gaussian noise with a zero mean and a standard deviation of 0.2 nT has been added. The contour interval is 2 nT.

away from the x - y -plane, most likely because the data are from a nonidealized model. We prefer to use a lower threshold value, in this case 0.7; this removes the effect of spurious 2D solutions resulting from noise in the eigenvectors while retaining 2D structures in areas clearly corresponding to this kind of structure in the 3D model (Figure 6e).

In practical terms, the parameterization of 2D-constrained grid Euler deconvolution (i.e., the choice of eigenvalue threshold and x - y -plane threshold values) is the main extra step involved in this method compared with the conventional grid

Euler method. Beyond this study, the obvious question to ask is: How easy is it to determine these parameters for a real data set? Preliminary studies show that 0.7 is a consistently good x - y -plane threshold value, removing the noisy 2D solutions. The eigenvalue threshold is less well defined, with sensible values varying by several orders of magnitude between different data sets. However, for each data set, finding the right order of magnitude is not time consuming, and then the process is simply fine-tuning to give the most coherent, geologically plausible pattern of 2D and 3D solution areas.

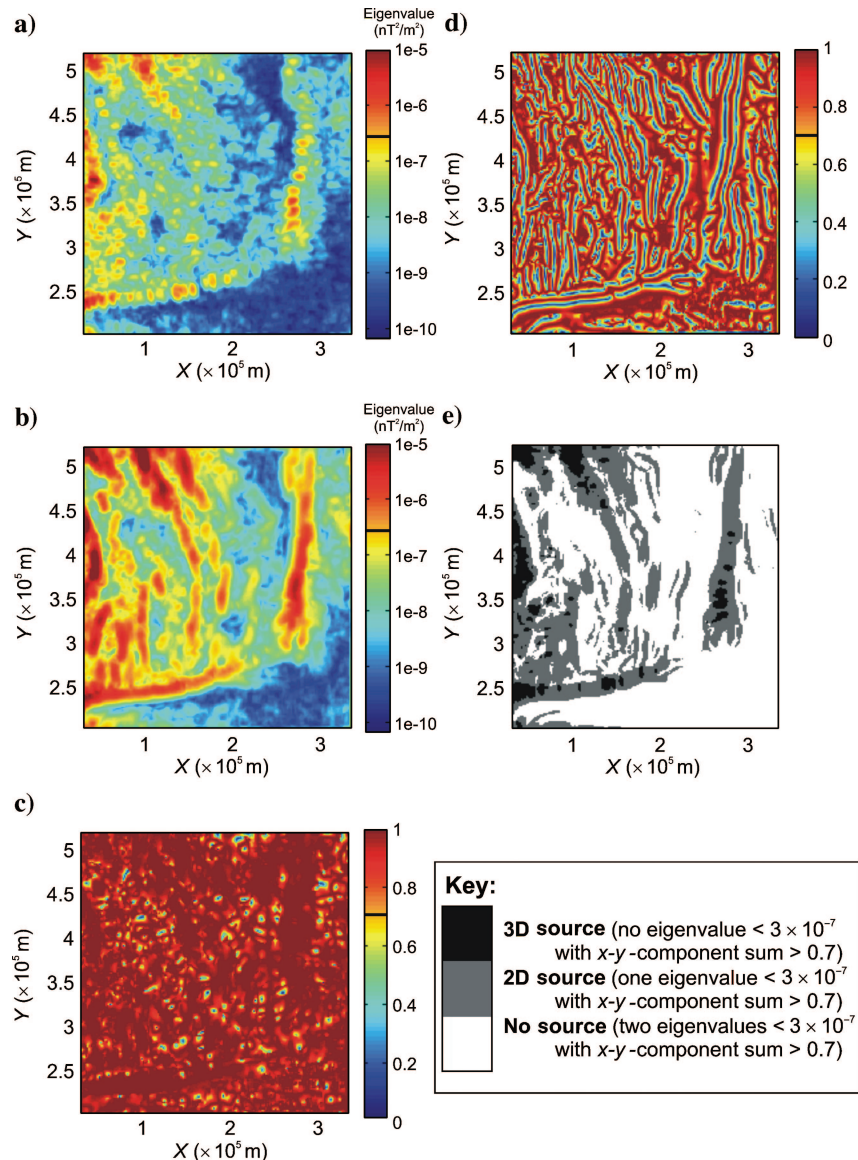


Figure 6. Eigenvalues and eigenvector information from the Euler $\mathbf{A}^T \mathbf{A}$ matrix for each window position in the Bishop model data. Black lines in color scale-bars indicate chosen threshold levels. (a) Smallest eigenvalue. (b) Second smallest eigenvalue. (c) Sum of x - and y -components of the eigenvector corresponding to the smallest eigenvalue. (d) Sum of x - and y -components of the eigenvector corresponding to the second smallest eigenvalue. (e) Spatial distribution of inferred structure type (3D, 2D, no source) in each window, using an eigenvalue threshold of 3×10^{-7} and an x - y -plane threshold of 0.7. Black areas indicate windows with 3D sources, gray indicates 2D sources, and white indicates no source.

Choice of structural index

Because we know the exact geometry of the model basement we are trying to image, we can directly compare this surface to the Euler solutions. Results were computed for a range of structural indices and compared with the true 3D model basement surface. Figure 7 is a histogram of the depth differences (3D model depth – Euler depth) for different structural indices associated with 2D sources. Depth difference in this case is defined as the vertical distance between a solution and the depth of the basement model interpolated to the same (x , y) coordinate; the (x , y) coordinate of a solution is normally well constrained compared to the depth (Ravat, 1996).

As we would expect, solutions for a single data set increase in depth with increasing assumed structural index (Reid et al., 1990). Figure 7 also shows that the zero-index solutions are typically too shallow, while an index of one produces solutions typically too deep. An index of 0.5 gives a histogram which peaks close to zero depth difference. In other words, the solutions for an index of roughly 0.5 typically give the most accurate depth estimations for our 3D basement model. [Reid et al. (1990) note that the structural index for faults varies between zero (for large throws) and one (for limited throws)]. Based on this analysis, the conventional and 2D-constrained grid Euler solutions should use a structural index of 0.5 for this data set, which is done in Figure 8a-f.

RESULTS

Euler solutions ($N = 0.5$)

Figure 8a shows all accepted solutions generated using the conventional grid Euler method. Figure 8b shows the corresponding depth differences (in modulus) between these solutions and the basement surface at the corresponding (x , y) position. Solutions with percentage depth errors (estimated from the least-squares inversion, as

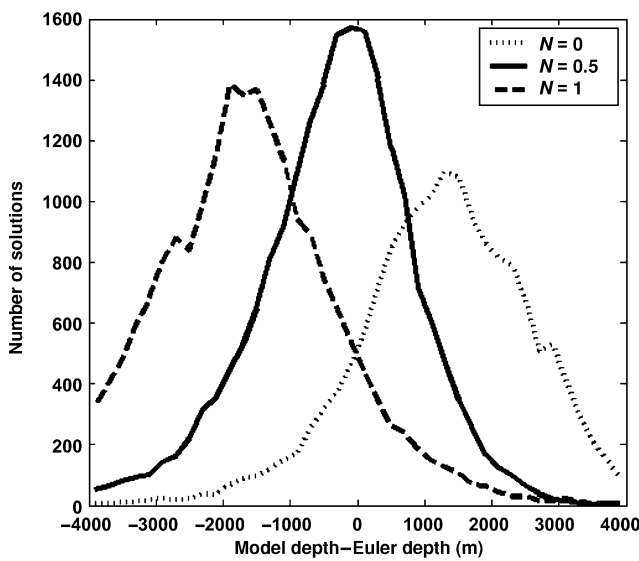


Figure 7. Histogram of 3D model depth – 2D constrained Euler depth values for Bishop model data, comparing different structural index values. Positive values indicate the solution is shallower than the model.

discussed in Methodology) greater than 3.7% are rejected. This chosen value gives the best balance between rejecting spurious, isolated solutions and keeping useful ones. For the 2D-constrained grid Euler method (Figure 8c and d) the optimum value for this criterion is 5%, a less severe value, although clearly fewer solutions are present because of additional solutions being rejected or considered three dimensional during the 2D-constrained grid Euler process. Therefore, we also include the results for conventional Euler rejecting solutions with a percentage depth error greater than 5% (Figure 8e and f). While these are not the optimum conventional grid Euler solutions, they represent a direct comparison between the conventional and 2D-constrained methods with the rejection criterion common to both methods set to the same level.

Both sets of solutions do a good job of imaging the structures in the model; solutions line up along the top edges of finite offset faults, which are responsible for the field anomalies. However, the conventional solutions include more additional, spurious solutions in areas where there are no obvious sources in the model (or anomalies in the data), whereas this is not seen in the 2D-constrained grid Euler solutions. Changing the rejection criteria to remove these unwanted solutions will also remove solutions within the clusters representing true

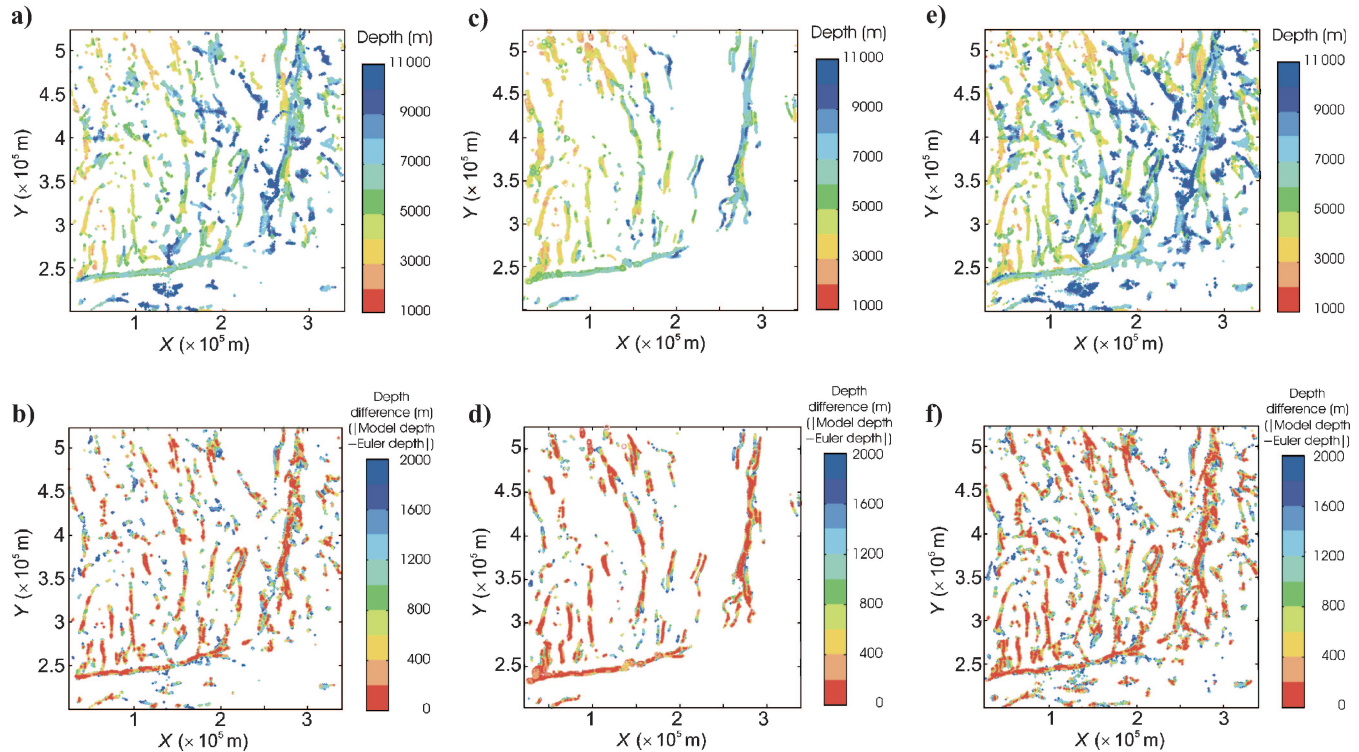


Figure 8. Euler deconvolution solutions for Bishop model data. (a) Conventional grid Euler solutions, with least-squares depth errors less than 3.7%. Colors represent solution depth. (b) Modulus difference in depth between the calculated (Euler) solutions in (a) and known (model) depth. (c) The 2D-constrained grid Euler solutions (dots) with least-squares depth errors less than 5%, colors representing solution depth. Conventional Euler solutions (also with a least-squares depth error less than 5%) from 3D source windows are shown as unfilled circles. (d) Modulus difference in depth between the Euler solutions in (c) and model depth. (e) Conventional solutions with least-squares depth errors less than 5%. Colors represent solution depth. (f) Modulus difference in depth between the Euler solutions in (e) and model depth.

structure. It is important to note that solutions which do not correspond to any topographic feature in the basement model and which have large depth errors can still occur in clusters. Thus, a cluster of solutions cannot be assumed to be correct just because it is a cluster. In the 2D-constrained grid Euler solutions, this problem does not occur because the clusters in question have been rejected. In these solutions, the clusters are predominantly along trends representing actual features in the model, with most depths consistent and close to the model depth at the same (x, y) position (close, in this case, means within 200 m vertically). Another important observation is that solution depths (from both Euler methods) vary

along linear trends, even where the depth of the corresponding source structure is roughly constant (e.g., Figure 8, $x = 185\,000, y = 360\,000$).

Statistical analysis of the results supports the view that the 2D-constrained grid Euler solutions define 2D sources more reliably than conventional Euler solutions. Figure 9a plots the number of points within each of the depth difference ranges shown in Figures 8b, 8d, and 8f as a percentage of the total number of solutions that have been accepted and plotted. Figure 9b shows the same depth differences as a percentage of the corresponding Euler depth. In both plots, the difference among the three curves illustrates the improved solution space generated by the 2D-constrained grid Euler method.

Figure 6e shows that windows considered three dimensional are generally adjacent to linear structures, where the overall linearity is disrupted by small breaks or undulations in the larger scale feature. Solutions in these windows (calculated using the conventional Euler method, shown as circles in Figure 8c and d) give good depth estimates when a structural index of roughly 0.5 is used. Normally, an N value of two (vertical pipe) or three (sphere) would be used, but the features in the model, while essentially three dimensional, do not conform to such geometries. Conventional Euler solutions calculated for the no-source windows do delineate some 2D features not picked up by 2D-constrained grid Euler deconvolution; for example, note a sharp break of slope trending northwest–southeast in the northeast section of the area (Figure 8, $x = 230\,000, y = 460\,000$). However, for these solutions, the structural index giving the best depth is highly variable, and it is unclear how the meaningful solutions could be identified.

DISCUSSION AND CONCLUSIONS

The implications of the results in this paper fall into two categories: the general idea of using appropriate topography data to provide a complex 3D basement test model for evaluating depth to basement estimators and the specific comparison between the conventional and 2D-constrained grid Euler methods using TMI data derived from this 3D test model.

Modeling strategy

In this study, our aim was to simulate magnetic data for a basin with nonmagnetic sediments overlying a faulted basement. If we accept that the assumptions made in the model are reasonable, then the results shown above are very useful in understanding how Euler deconvolution results relate to real geology and what level of resolution is realistically achievable. Our results demonstrate that a structural index of roughly 0.5 gives the most accurate depth estimates for data where the typical source structures are finite-offset faults/steps. An index of 0.5 presents theoretical problems; model studies have demonstrated that for structures with an index of around 0.5, the exact index varies spatially (i.e., from window to window and within a solution window), leading to potential inaccuracies (Ravat, 1996) — a problem not encountered when using integer structural indices. However, the results of our study show that while such inaccuracies may be present, the depth estimates are nonetheless closer to the model depth using a noninteger index.

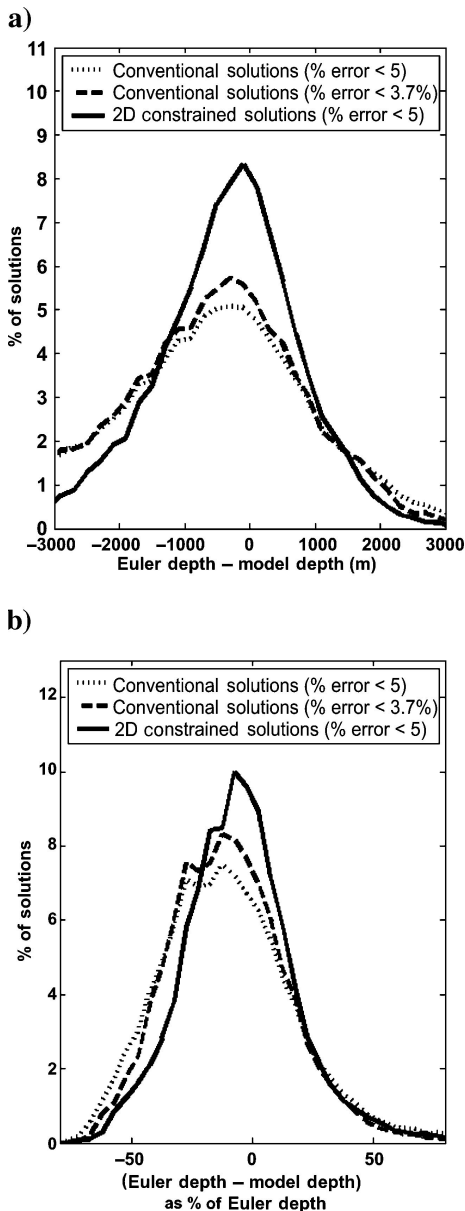


Figure 9. Histograms showing the percentage of the total number of accepted solutions for the conventional and 2D-constrained Euler solutions (a) within given ranges (2D-constrained Euler depth – 3D model depth) and (b) within ranges based on these depth differences as a percentage of the Euler depth.

Even using the optimal structural index and with poor solutions rejected, some solutions remain with large depth errors. These solutions often occur as part of a cluster of generally reliable solutions and highlight the importance of interpreting source depths based on solution clusters rather than individual solutions. Solution trends appearing to show along-strike variations in source depth should be treated with caution, as they may be from poor depth estimation.

Euler method comparison

Our comparison of different Euler methods reveals that, when compared with conventional grid Euler methods, 2D-constrained solutions are less scattered, more laterally continuous along linear structures, and more consistently close to the true depth of the structures they are imaging. The cleaner solution pattern produced by the 2D-constrained technique is largely attributable to solutions from windows with no distinct source being rejected. The 2D-constrained solutions do not image curved fault traces, fault tips, and intersections of crosscutting features. These are identified as 3D source areas, and such solutions are generated using conventional Euler methods.

The 2D-constrained methodology allows us to classify the likely source geometry in each Euler solution window. The results here suggest that in study areas where dikes and/or contacts are present (not the case in our model), 2D-constrained Euler methods could provide a means of calculating dip and susceptibility contrast while also allowing 3D structures to be treated with a different structural index. Thus, the 2D-constrained Euler deconvolution provides a new approach to estimating magnetic source-depth in areas where all or some of the sources are two dimensional.

Further work

This study presents great potential for further work. The 3D model can be used to quantitatively compare and contrast different methods of depth-to-basement estimation, as well as transformation (e.g., RTP operators). Our model is still relatively simple and will be adapted to incorporate variations in basement susceptibility, intrasedimentary volcanics, or geological/survey noise. The same methodology could also be applied to topography data from other areas where the surface exposed structures are good analogs to sedimentary basins.

ACKNOWLEDGMENTS

We are grateful to J. B. C. Silva, J. B. Thurston, and B. Kulessa for their insightful reviews, which led to significant

improvements in this manuscript. We also thank A. B. Reid for his continued advice and encouragement and A. J. Carter and M. Felix for valuable discussions. The topography data are from the U. S. Geological Survey (USGS) and are freely available on the Internet (contact J. D. F. or G. F. for further details). The forward modeled grids were generated using Fugro's 3MOD software, which calculates a field composed of a series of magnetized layers using a proprietary fast Fourier transform technique. S. E. W. is supported by research grants from ConocoPhillips and the University of Leeds.

REFERENCES

- Barbosa, V. C. F., J. B. C. Silva, and W. E. Medeiros, 1999, Stability analysis and improvement of structural index estimation in Euler deconvolution: *Geophysics*, **64**, 48–60.
- Fairhead, J. D., K. J. Bennet, D. R. H. Gordon, and D. Huang, 1994, Euler: Beyond the “Black Box”: 64th Annual International Meeting, SEG, Expanded Abstracts, 422–424.
- Gunn, P. J., 1997, Quantitative methods for interpreting aeromagnetic data: A subjective review: *Journal of Australian Geology & Geophysics*, **17**, 105–113.
- Hsu, S.-K., 2002, Imaging magnetic sources using Euler’s equation: *Geophysical Prospecting*, **50**, 15–25.
- Mushayandebvu, M. F., V. Lesur, A. B. Reid, and J. D. Fairhead, 2004, Grid Euler deconvolution with constraints for 2D structures: *Geophysics*, **69**, 489–496.
- Mushayandebvu, M. F., P. van Driel, A. B. Reid, and J. D. Fairhead, 2001, Magnetic source parameters of two-dimensional structures using extended Euler deconvolution: *Geophysics*, **66**, 814–823.
- Nabighian, M. N., and R. O. Hansen, 2001, Unification of Euler and Werner deconvolution in three dimensions via the generalized Hilbert transform: *Geophysics*, **66**, 1805–1810.
- Naudy, H., 1971, Automatic determination of depth on aeromagnetic profiles: *Geophysics*, **36**, 717–722.
- Phillips, J. D., 2002, Two-step processing for 3D magnetic source locations and structural indices using extended Euler or analytic signal methods: 72nd Annual International Meeting, SEG, Expanded Abstracts, 727–730.
- Ravat, D., 1996, Analysis of the Euler method and its applicability in environmental magnetic investigations: *Journal of Environmental and Engineering Geophysics*, **1**, 229–238.
- Reid, A. B., J. M. Allsop, H. Granser, A. J. Millett, and I. W. Somerton, 1990, Magnetic interpretation in three dimensions using Euler deconvolution: *Geophysics*, **55**, 80–91.
- Roest, W. R., V. Verhoef, and M. Pilkington, 1992, Magnetic interpretation using the 3-D analytic signal: *Geophysics*, **57**, 116–125.
- Spector, A., and F. S. Grant, 1970, Statistical models for interpreting aeromagnetic data: *Geophysics*, **35**, 293–302.
- Thompson, D. T., 1982, EULDPH: A new technique for making computer-assisted depth estimates from magnetic data: *Geophysics*, **47**, 31–37.
- Werner, S., 1953, Interpretation of magnetic anomalies of sheet-like bodies: *Sveriges Geologiska Undersökning, Årsbok* **43**(1949), No. 6.
- Williams, S. E., J. D. Fairhead, and G. Flanagan, 2003, Grid-based Euler deconvolution: Completing the circle with 2D constrained Euler: 73rd Annual International Meeting, SEG, Expanded Abstracts, 572–575.

